Atmos. Chem. Phys. Discuss., 12, 24395–24435, 2012
www.atmos-chem-phys-discuss.net/12/24395/2012/
doi:10.5194/acpd-12-24395-2012

Atmospheric Chemistry and Physics Discussions

Black carbon concentration and deposition estimations in Finland by the regional aerosol-climate model REMO-HAM

A. I. Hienola[1], J.-P. Pietikäinen[1], D. Jacob[2,3], R. Pozdun[2,3,†], T. Petäjä[4], A.-P. Hyvärinen[1], V.-M. Kerminen[4], M. Kulmala[4], and A. Laaksonen[1]

[1]Finnish Meteorological Institute, Erik Palmenin aukio 1, 00101, Helsinki, Finland
[2]Max Planck Institute for Meteorology, Bundersstrasse 53, 20146 Hamburg, Germany
[3]Climate Service Center, Chilehaus – Eingang B, Fischertwiette 1, 20095 Hamburg, Germany
[4]Department of Physics, Division of Atmospheric Sciences and Geophysics, University of Helsinki, P.O. Box 64, 00014 University of Helsinki, Finland
[†]deceased, September 2011

Received: 23 July 2012 – Accepted: 3 September 2012 – Published: 18 September 2012

Correspondence to: A. I. Hienola (anca.hienola@fmi.fi)

Published by Copernicus Publications on behalf of the European Geosciences Union.

Abstract

The prediction skill of the regional aerosol-climate model REMO-HAM was assessed against the black carbon (BC) concentration measurements from five locations in Finland, with focus on Hyytiälä station for the year 2005. We examined to what extent the model is able to reproduce the measurements using several statistical tools: median comparison, overlap coefficient OVL (the common area under two probability distributions curves) and Z-score (a measure of standard deviation, shape and spread of the distributions). The results of the statistics showed that the model is biased low, suggesting either an excessive loss of black carbon in the model, or missing emissions. A further examination of the precipitation data from both measurements and model showed that there is no correlation between REMO's excessive precipitation and BC underestimation. This suggests that the excessive wet removal is not the main cause for the low black carbon concentration output. In addition, a comparison of wind directions in relation with high black carbon concentrations shows that REMO-HAM is able to predict the BC source directions relatively well. Cumulative black carbon deposition fluxes over Finland were estimated, including the deposition on snow.

1 Introduction

Black carbon (BC), operationally defined as the light absorbing fraction of carbonaceous aerosols, is an air pollutant formed through the incomplete combustion of fossil fuels, biofuel, and biomass, and is emitted in both anthropogenic and naturally occurring soot (Cooke et al., 1999). Soot particles absorb solar radiation, causing an increase in their temperature and emission of thermal-infrared radiation into the surrounding space. When BC deposits onto a frozen surface, such as snow or ice, the immediate effects are changing the reflectivity of the snow and heating the surface, both of them promoting ice and snow melting (Jacobson, 2004; Hansen and Nazarenko, 2004). Deposition of "soot on snow" is thought to affect the climate on regional and

ACPD
12, 24395–24435, 2012

global scales. Jacobson (2004) predicted a reduction in snow albedo due to BC deposition of 1 % in the Northern Hemisphere and 0.4 % globally, assessing and increase in global temperature of 0.06 °C. Hansen et al. (2005), based on a simulated deposition of BC, parametrized the changes in snow albedo, calculated a positive radiative forcing of 0.15 W m^{-2} and estimated a global warming of 0.24 °C.

Due to the numerous and complex mechanisms through which BC affects the radiation balance, estimating the impact of black carbon on climate change remains largely uncertain. As black carbon has a relatively short lifetime in the atmosphere (a couple of days to less than 2 weeks), it has been considered as a candidate species for immediate reduction of climate forcing, as part of short-term climate control strategies (Levy et al., 2008; Bond et al., 2011). Therefore, proper BC modelling is needed and stands out as of great interest among atmospheric scientists. However, model simulation of BC is hindered by various factors. For instance, accurate knowledge of BC emissions is essential for a proper model-prediction of black carbon. Global BC emission inventories show large discrepancies due to differences in emission factors and sources. According to Bond et al. (2004), emission inventories can have an uncertainty of a factor of 2, while Ramanathan and Carmichael (2008) give a factor of two to five on regional scale, and a minimum of ±50 % on global scale. These uncertainties play an even more significant role in regional simulations, as at smaller scale the actual emissions are more likely to deviate even more from the annual or monthly mean inventory.

In addition to the uncertainties due to the inaccuracy of the input data, current models – whether global or regional – are still agonizing due to the great difficulties in representing the complexities of aerosol dynamics (and in this particular case, the evolution of BC) in a rigorous way. Vignati et al. (2010b) underlined the importance of an adequate characterization of the black carbon aging process in the models. After being emitted to the atmosphere, BC goes through a series of chemical and physical transformations. Condensation of soluble material onto BC, coagulation of BC particles with soluble particles and photochemistry are contributing processes collectively known as aging. The aging process should not be overlooked, as it changes

ACPD
12, 24395–24435, 2012

the particles' composition and hence their physico-chemical properties (Furutani et al., 2008; Decesari et al., 2006). For instance, the particle's hygroscopicity is modified from a hydrophobic state towards a more hydrophilic state. The hygroscopicity of BC defines which removal process – wet or dry deposition – will be more effective, and hence impacting the black carbon lifetime by an estimated one order of magnitude (Croft et al., 2005). Observations have shown that wet deposition represents 70–85 % of the tropospheric sink for the carbonaceous aerosols (Pöschl, 2005). However, wet deposition is considered one of the most uncertain process in models (Textor et al., 2006).

To date, many global models have been used to study the spatial and temporal evolution of BC particles, as well as their physical properties. In early attempts to model black carbon concentrations, modellers assumed that BC was externally mixed and had a constant size distribution (Haywood and Shine, 1995; Tegen et al., 1997). More up-to-date models include BC size fractionation and internal mixing (Stier et al., 2005; Vignati et al., 2010a; Schwarz et al., 2010; Gilardoni et al., 2011). For a very comprehensive overview of the BC simulation, the reader is directed to Koch et al. (2009), who compared seventeen models from the Aerocom aerosol model comparison with several types of observation, revealing large BC discrepancies, coming mostly from BC inventories and from the models' characteristics.

Although numerous regional climate models exist, few have been used to analyze black carbon distribution and properties. Carmichael et al. (2003) used the regional scale transport model CFORS to calculate BC concentrations (among other species) and presented a comparison with aircraft measurements above Asia. Using the same model, Uno et al. (2003) went into a more detailed analysis of black carbon, using surface BC measurements at five remote Japanese islands for model validation. In both cases, the CFORS model seemed to underestimate black carbon levels. Wu et al. (2004) investigated the emission, transport and distribution of black carbon-containing aerosols and their radiative effect over China by means of the regional climate model RIEMS. Solmon et al. (2006) implemented a simplified anthropogenic aerosol model within the regional climate model RegCM and ran it over a large domain extending from

ACPD
12, 24395–24435, 2012

northern Europe to south tropical Africa. The model evaluation was carried out in terms of black carbon, organic carbon and sulphate surface concentrations and aerosol optical depths. More recently, Wu et al. (2008), using Regional Climate Model RegCM3 simulated the direct radiative effects of BC over the Asian region and investigated the possible climate change induced by BC. However, the authors, among other simplifications, considered in their model only black carbon as such, without any internal or external mixing with other kind of aerosols.

To the authors' knowledge, no other regional model studies regarding black carbon have been conducted in the recent years. The lack of interest in the subject is surprising, given the fact that regional models – with their relatively higher resolutions – could bring an enhanced understanding of the behaviour of BC aerosols and their climatic impact on regional scale.

In this study we apply and explore the performance of our current version of regional aerosol-climate model REMO-HAM in terms of black carbon near-surface concentrations and deposition fluxes in Finland. The authors stress the fact that this work is only the first step towards a more comprehensive development effort of the present regional climate model.

The outline of the article is as follows: a brief description of the model, the sites and the instrumentation is given in Sect. 2. Section 3 deals with the comparison between observations and the model results, several statistics with the focus on Hyytiälä station and estimations of total deposition fluxes and deposition on snow over Finland, and Sect. 4 summarizes the results and draws conclusions.

2 Model description and experiments

2.1 REMO-HAM model

The regional climate model REMO is a hydrostatic, three-dimensional atmospheric model developed at the Max Planck Institute for Meteorology in Hamburg and based

ACPD
12, 24395–24435, 2012

on the Europa Model, the former numerical weather prediction model of the German Weather Service (Jacob and Podzun, 1996; Jacob, 2001). The physics of the model is derived from the global circulation model ECHAM4 (Roeckner et al., 1996), although many parts have been changed due to higher resolution. Moreover, the model has been updated so that the physics is partly based on ECHAM5 (Roeckner et al., 2003; Pietikäinen et al., 2012).

Pietikäinen et al. (2012) implemented the aerosol module HAM-M7 to the REMO model. HAM-M7 is an aerosol chemistry and physics module, which predicts the evolution of an ensemble of microphysically interacting internally- and externally-mixed aerosol population as well as their size-distribution and composition (Vignati et al., 2004). The size-distribution is represented by a superposition of seven log-normal modes: one soluble nucleation mode, together with soluble and insoluble aitken, accumulation and coarse modes. The M7 microphysical core includes coagulation, condensation of sulphuric acid gas, nucleation, thermodynamical equilibrium with water vapor and redistributes the particle mass and number between modes (Stier et al., 2005). The aerosol components considered in HAM-M7 are sulphate (S), black carbon (BC), particulate organic carbon (POM), sea salt (SS) and mineral dust (DU). Table 1 summarizes the way HAM-M7 treats different species and how the aerosol components are divided between different modes. Black carbon is defined in soluble and insoluble Aitken modes and in soluble accumulation and coarse modes. The aging is achieved via condensation of sulphuric acid and coagulation with soluble particles. When condensation of sulfate forms a soluble monolayer on the surface of the hydrophobic BC aerosols, they are moved from insoluble to soluble/mixed mode (Vignati et al., 2004). Similarly for coagulation: when a soluble mode particle coagulates with an insoluble one, the resulting particle is assumed to be soluble. Within the soluble and insoluble modes, the growth of particles can lead to inter modal transfer (Stier et al., 2005).

The aerosol module has been coupled with a stratiform cloud scheme, but so far it has not been coupled with radiation (Pietikäinen et al., 2012).

ACPD
12, 24395–24435, 2012

BC (and other species) undergoes different transport processes in the model: transport in convective clouds, dry- and wet deposition, sedimentation, vertical diffusion and vertical- and horizontal advection (Stier et al., 2005; Pietikäinen et al., 2012). The convective transport of tracers is based on the mass-flux scheme by Tiedtke (1989) with modifications by Nordeng (1994). The dry deposition is built on the same size-dependent parametrization as in the ECHAM5-HAM, and the wet deposition is based on the size dependent below-cloud scavenging scheme by Croft et al. (2009). The sedimentation velocity calculation is based on the Stokes velocity with the Cunningham slip-flow correction factor accounting for non-continuum effects (Stier et al., 2005). The sub grid scale vertical diffusion fluxes are calculated according to Louis (1979) for the lowest level. For other levels, the model uses a second-order closure scheme of hierarchy level 2 by Mellor and Yamada (1974). The horizontal and vertical advection is solved with a finite difference, antidiffusive scheme by Smolarkiewicz (1983, 1984).

The emissions used in the present study are based on AEROCOM emission inventory for the year 2000 (http://nansen.ipsl.jussieu.fr/AEROCOM/), except for the sea salt and dimethyl sulphide (DMS) emissions which are based on an approach by Stier et al. (2005). BC emissions originate from three different sources: vegetation fires, usage of fossil-fuels and usage of bio-fuels. All black carbon emissions are released to the insoluble Aitken mode. A detailed list of other different emission species and sources is presented in Dentener et al. (2006).

2.2 Experimental data

The measurements were conducted at five different locations in Finland: Pallastunturi GAW (Global Atmosphere Watch) station (Hatakka et al., 2003), Hyytiälä SMEAR II (Station for Measuring Forest Ecosystem – Atmosphere Relations) station (Kulmala et al., 2001; Hari and Kulmala, 2005), Puijo SMEAR IV station (Leskinen et al., 2009), Utö EMEP (European Monitoring and Evaluation Programme) station (Engler et al., 2007) and Virolahti EMEP station (Anttila et al., 2008). The measurement sites and instruments have been described in detail by Hyvärinen et al. (2011) and are presented

ACPD
12, 24395–24435, 2012

in Fig. 1. The color scheme in the figure depicts the black carbon annual emissions in the model domain.

The black carbon measurements were conducted with two different instruments: the AE 31 aethalometer (Magee Scientific) and the multi angle absorption photometer (MAAP) (Thermo Scientific). As BC by definition cannot be unambiguously measured with these instruments, it is customary to call the measured light absorbing constituent as equivalent BC. As both the aethalometer and MAAP utilize a light absorbance method on a filter strip, they yield very comparable data of the aerosol BC, as was found at Pallastunturi (see supplementary material in Hyvärinen et al., 2011).

The measurement details of BC from each station are specified in Table 2. The concentrations measured behind different inlets are comparable as long as there are no sources of primary soot from e.g. incomplete combustion (Hyvärinen et al., 2011). The measurement resolution of the instruments was typically one minute. Five-minute average data were quality-checked and data with outliers or instrument problems were removed. More than 20 min of data coverage was required for the computation of hourly averages.

3 Results

To characterize the REMO-HAM's abilities and limitations, the model results calculated for the year 2005 are compared with experimental data. This study uses observations from five sites for different periods of time as specified in Table 2. For each site we used the first full year with available data. According to Hyvärinen et al. (2011) BC concentrations exhibited a clear seasonal cycle with the highest concentrations during the spring and winter, and the lowest during the summer. As such, the comparison of the 2005 model run with different years of experimental data should be regarded as qualitative rather that quantitative in nature. Because Hyytiälä station had black carbon measurements for the entire 2005, the analysis and the comparison will focus on this station only, while for the others we will just briefly summarize the findings.

ACPD
12, 24395–24435, 2012

The BC concentration measurements are punctual, while the model gives the parameter over an area defined by the model's grid box. However, since the resolution used in REMO is 0.44° × 0.44° (50 × 50 km^2) and there are no major point sources within the grid cells (Williams et al., 2011), we can consider that the point measurement is representative for the entire grid cell. The BC concentrations at given location were calculated using the CDO remapping tools, that is, a bilinear interpolation to a one-point grid in which the coordinates (latitude and longitude) have been defined.

3.1 BC concentrations: model vs. measurements

The surface mass concentrations of black carbon were examined first. The monthly means of modelled and measured black carbon concentration for the 5 station are shown in Fig. 2. A seasonal variation is detected for all the stations, with a maximum in late winter/early spring and a second maximum in the autumn, potentially due in part to lower mixing height levels during this time of the year. The model was able to reproduce the seasonal cycle to a certain extent. In all cases, the model agreed better with the measured values outside of the periods of maximum observed BC concentrations.

At Hyytiälä, the observed monthly mean concentrations ranged from 175 to 687 ng m^{-3}, while the modeled monthly means ranged from 100 to 334 ng m^{-3}. REMO underestimated the observations significantly during the winter and autumn maxima by more than 50 %. During early spring and summer, the disagreement between REMO results and observations was still quite high, with an average underestimation of roughly 40 %.

The highest monthly averaged concentrations measured in Pallas was 160 ng m^{-3} during February and 143 ng m^{-3} during March. The autumn maximum was less pronounced in comparison to the other locations. REMO seriously underestimated the observations during July–September, when modelled BC was about 20 % of the measured BC. The model overestimated the observations during October by 22 %.

ACPD
12, 24395–24435, 2012

At Puijo, the measured monthly average concentrations were in the range of 114–445 ng m^{-3}. REMO underestimated the observed monthly averages by 31 %, the largest differences seen in August (67 %) and September (61 %).

The BC experimental monthly means in Virolahti varied from 225 to 707 ng m^{-3}. The corresponding range was simulated by REMO as 70–426 ng m^{-3}. On average, REMO underestimated the observations by 50 %.

The measurements at Utö showed a clear maximum in March, which was not captured by the model. However, REMO reproduced the measurements quite well for most of the months, with the exception of March, August and December, when the differences between the model results and observations were considerable.

Overall, a systematic underestimation of calculated black carbon concentrations was detected for all stations, with pronounced problems during February and March, followed by less pronounced discrepancies during the autumn.

3.2 Case study: Hyytiälä

3.2.1 Statistics

Figure 3 depicts the box-and-whisker monthly diagram of 3-hourly resolution data of modelled (upper panel) and measured (lower panel) black carbon concentrations. In each box, the central solid red line locates the median, the edges of the box are the lower and upper quartiles (25th and 75th percentiles), the whiskers stretch to the most extreme data points that were not considered outliers, and outliers are shown individually (red plus mark). The REMO outliers were relatively evenly distributed, except for January and May, while the measurements showed more variability in the extreme values. Both REMO and measurement monthly data were positively skewed (with a long upper whiskers and a large number of outliers towards larger values), showing a strong departure from the normal Gaussian curve. As such, the use of median instead of mean makes more sense for comparing the time series of the model and the measurements. The same figure shows distinctly different upper extreme values, or,

ACPD
12, 24395–24435, 2012

in other words, different concentration ranges. The REMO concentrations went up to about 1200 ng m^{-3}, while the measurements reached values up to 3000 ng m^{-3}.

For further comparison, the monthly medians are presented in Fig. 4. The highest measured monthly median value appeared in February, which was about 2–3 times higher than observed during the rest of the months. This pattern is consistent with other measurements made in Hyytiälä during 2006–2008 presented in Hyvärinen et al. (2011) (Fig. 3/panel 3 in their article), except for 2008 when the median BC concentration peaked in March. The largest discrepancy between the model and the measurements was also recorded in February, with a modelled median BC concentration being about 3.5 times smaller than the measured median. On the other hand, March and September showed the best agreement between the model and the measurements in terms of medians, while for the rest of the months the simulated values were within a factor of 2 of the corresponding measured values.

The scatterplot of 3-h resolution data for the entire period presented in Fig. 5 gives a good visual picture of the less-than-perfect correspondence between the two sets of data. The model underestimate is evident. It is difficult to point out a specific reason for this underestimation. However, the February case seems to be a local feature, where the probable cause is the existence of a point BC source not accounted for in the model's emission inventory. The local emissions affect BC concentrations on short time scales and consequently induce larger variabilities of observations as compared to model simulations. REMO's constant under-predictive capability suggests also a problem in the BC wet removal scheme.

The use of a single statistic (like median) to gauge the quality of the model is dangerous and usually insufficient. In order to asses the agreement between the model and the observations, several other statistical tools should be considered. For instance,the overlap coefficient (OVL*), defined as the common area under two probability distributions curves, offers an attractive technique for exploring the discrepancies between two samples and provides a good measure of the agreement between the distributions. In

ACPD
12, 24395–24435, 2012

general, this area is defined as:

$$\mathrm{OVL}^{*} = \int_{-\infty}^{\infty} \min[f_1(X), f_2(X)]\,\mathrm{d}X, \quad (1)$$

where $f_1(X)$ and $f_2(X)$ are the probability density functions of the two distributions (Clemons and Bradley Jr., 2000). In our case, the overlap coefficient is calculated by dividing OVL^{*} by the area under the measurements PDF, resulting in a fraction (or percentage, respectively, if multiplied by 100) of the measurements that are covered by the model. Henceforth, this fraction will be denoted by OVL. OVL ranges from 0 – when the distributions are completely distinct – to 1, when the distributions are identical. Like any other statistical tool, OVL has its own advantages and disadvantages. On the plus side, OVL is a simple, easy-to-understand concept, as well as less restrictive than other methods, in the sense that the measurement of the agreement between the distributions can be done no matter what the distribution setting is. The disadvantage of using OVL lies in the fact that its magnitude does not denote where the common area is located.

Our distributions were positively skewed and therefore a reasonable parametric form to characterize them was hard to deliver. As such, we considered a nonparametric approach, in the form of a kernel density estimator. Figure 6 depicts the histograms and the nonparametric density functions for the measured and computed 3-hourly resolution black carbon concentrations for Hyytiälä over the entire year 2005. The model distribution data was narrow and shifted towards smaller concentrations, whereas the measurement distribution had a long tail towards higher concentrations. In this case, the overlapping coefficient was 0.59, showing that nearly 60 % of the observed data could be explained by the model. However, the model failed to simulate concentrations higher than about 500 ng m^{-3} and underestimated the concentrations between 250 and 500 ng m^{-3} by more than 50 %. For very low concentrations the model overestimated the observations significantly.

ACPD
12, 24395–24435, 2012

More information about REMO-HAM behaviour can be obtained by exploring the monthly density functions presented in Fig. 7 together with the monthly overlap of the probability density curves (blue) and the monthly Z-score from Mann-Whitney U test shown in Fig. 8. In terms of the overlap coefficient, the poorest agreement between REMO and measurements was observed in February, with an OVL less than 0.4 – as expected from the median comparison in Fig. 4, while for the rest of the months the agreement was constantly above 0.5. The highest overlap values were registered in March and September with values above 0.8, followed by May, October and November with OVLs between 0.7 and 0.8. In terms of seasons, the model was able to explain 76 % of the observed data for autumn, 72 % for spring, 59 % for summer and only 48 % for winter. There was no seasonal pattern associated with the overlap coefficient.

The Mann-Whitney U-test is the non-parametric equivalent of, and with a similar statistical power as, the independent samples t-test. It is used when the sample data are not normally distributed. The Mann-Whitney U-test is applied to the 3-h resolution data from the measurements (M) and REMO (R). First, the data were combined into a set of $N = N_M + N_R$ elements (the number of measurement and REMO data points), then ranked from lowest to highest, including tied rank values where appropriate. The rankings were re-sorted into the two separate samples R and M and the sum of the ranks of each sample (S_R and S_M) was calculated. The Mann-Whitney U statistic is given by:

$$U = \min(U_M, U_R), \tag{2}$$

where the U statistic for each sample is

$$U_i = S_i - \frac{N_i(N_i+1)}{2}, \tag{3}$$

with i = R, M. For a large sample ($N > 20$), the normal approximation or the Z-score (or coefficient) can be calculated as

$$Z = \frac{\left|\frac{N_R N_M}{2} - U\right|}{\sigma}, \tag{4}$$

ACPD
12, 24395–24435, 2012

where σ is the standard deviation given by

$$\sigma = \sqrt{\frac{N_R N_M (N+1)}{12}}. \quad (5)$$

In case two or more data are the same, the normal approximation still can be used with an adjustment to the standard deviation

$$\sigma = \sqrt{\frac{N_R N_M}{N(N-1)} \left[\frac{N^3 - N}{12} - \sum_{j=1}^{g} \frac{t_j^3 - t_j}{12} \right]}, \quad (6)$$

where g is the number of groups of ties and t_j is the number of tied ranks in group j.

The Z-score is a measure of standard deviation, but also a test of statistical significance that helps to decide whether or not to reject the null hypothesis. The null hypothesis is in principle an hypothesis of "no difference". Very high Z-scores are usually found in the tail of a distribution, indicating that the null hypothesis is very unlikely. In our case, large values of Z were associated with poor agreement between the observations and the model results. According to Fig. 8, only one Z-value was below the usually agreed critical Z-score value of 1.96 (corresponding to 95 % confidence level), that is in case of March, which also corresponds to a large overlap coefficient. This is the only case when we can not reject the null hypothesis. The Z-scores for the rest of the months ranged from 2.5 to 12, indicating that a rejection of the null hypothesis is possible. As expected, the Z-score and the overlap coefficients were anti-correlated. However, in some cases, a relatively high OVL was characterized also by high Z-values (see May, August, October and November). The highest Z-scores (above 9) were found for January, February, July and December and were related also to clearly different shapes of the model and measurement distribution curves. According to Hart (2001), the Mann-Whitney test (and the related Z-score) can detect not only the differences in medians, but also the differences in shapes and spreads.

ACPD
12, 24395–24435, 2012

3.2.2 Wind direction and black carbon concentrations

Hourly wind direction data for Hyytiälä were obtained from http://www.atm.helsinki.fi/~junninen/smartSearch (Junninen et al., 2009) and then combined on a 3-h basis to match the corresponding modelled data. In order to determine the wind direction conditions contributing to the highest BC concentration levels in Hyytiälä, the black carbon concentrations were categorized by wind direction. Figure 9 presents the wind-rose diagram and the associated measured BC concentrations for each season. The length of the slices represents the percentage of time the wind blows from a certain direction and the color diagram represents the black carbon mass concentration. The prevailing wind direction was from the south. However, the diagram indicates that the major black carbon contribution came from south-east and south-south-east corridors which were also associated with low wind speeds (not shown). These directions hint Orivesi as the dominant source. Orivesi is a typical Finnish town, with a population of approximately 10 000, located 20 km from Hyytiälä, consisting mostly of houses, with no significant industrial activity. In such towns, the residential wood burning is considerable all around the year, a BC source usually overlooked in the (global) emission databases.

The second highest concentrations of black carbon came from the the south-west sector, mostly evident in autumn, but less distinct during spring and winter. A possible source in this direction is Tampere (population of 213 000), the largest inland city in the Nordic countries located about 60 km from Hyytiälä. Although Tampere is definitely a stronger source of black carbon than Orivesi, the concentrations measured from this direction were smaller, potentially due to the greater distance and to higher wind speed, the latter affecting the BC concentrations through its dispersive effects.

The modelled wind directions and their associated black carbon concentrations are presented in Fig. 10. Although the model fittted well the measurements during the autumn, the correlation between the model data and the observations in Hyytiälä for the entire year 2005 was rather low. This is most likely due to the fact that the wind direction measurements represented real local conditions, while the model results were

ACPD
12, 24395–24435, 2012

the values from the edges of the grid box of the location. However, the directions of the highest concentrations of black carbon, although not as elevated as in the measurement data, were reproduced fairly well by the model. The omnipresent exception was found in spring, when elevated concentrations of BC came from north-east sector, fact that did not appear in the measurements. This may hint to the missing residential wood-burning source as the main contribution to the model underestimates.

3.2.3 Precipitation and black carbon concentrations

Wet removal is the dominant sink for the black carbon and thus a potential cause for the underestimated black carbon concentrations. We compared the model results against measurement data from CRU TS 3.0 (Jones et al., 2008). The CRU TS 3.0 dataset is available on a 0.5 degree grid, has a monthly time resolution, and covers all the land points of Earth. The precipitation data from REMO-HAM were conservatively remapped to the CRU grid so that a direct comparison is possible.

The monthly comparison of precipitation in Southern Finland is presented in Fig. 11 as a percentage difference between the model output and the measurements. The blue color marks the model overestimatimation of precipitation, which seemed to occur during each month, preponderantly in January, March, April, May, June and December. The red color depicts model underestimation and the area mean on top of each plot represents the mean precipitation difference around Hyytiälä. There was no obvious correlation between REMO's excessive precipitation and REMO's black carbon underestimation. If the wet removal were the leading reason for the black carbon underestimation, we would expect a high percentage difference in precipitation during February (area mean of just 26 %), when the BC underestimation was highest, or a good agreement in precipitation in March (area mean of 110 %), when also the BC concentrations matched. The same reasoning can be applied for the remaining months: for April to August the REMO BC underestimation was similar, while the precipitation difference given by the area mean ranged from 26 % in June to 198 % in April. The only agreement between precipitation difference and BC underestimation was found

ACPD
12, 24395–24435, 2012

in September, when both of the above quantities were small. It is possible that the overestimated precipitation might contribute to a certain extent to the underestimation of BC concentrations. However, because no monthly correlation was observed suggests that the low BC fluxes in the emission inventories are the main reason for BC underestimation rather than the model overestimating the wet removal.

3.3 Modelled black carbon concentration and deposition over Finland

The continuous REMO-HAM simulation for the year 2005 delivers a complete annual cycle of the black carbon concentration and deposition over the entire Finland. Figure 12 presents the modelled near-surface BC median concentrations for all seasons. Each spatial figure exhibits a similar pattern: a clean Northern Finland atmosphere, with increasing black carbon concentrations as moving southwards, reaching a maximum around the city of Helsinki. The spatial distribution of black carbon concentration corresponds to high emission regions with high population density (see Fig. 1 for comparison). The same figure reveals that the BC concentration is lower during the summer than during the other seasons over most of the domain. Given the results obtained by comparing the observed and modelled BC concentrations in various locations around Finland, we can assume that the real concentrations values for the entire domain will exceed the model estimates by approximately a factor of two.

Figure 13 presents the total black carbon deposited during each season.The spatial distribution of the total deposition was correlated to the black carbon emissions (Fig. 1) and had a strong geographical and temporal variability: the largest deposition occurs in the higher populated regions, that is, in Southern and central Finland, while Northern Finland had the lowest deposition rate, due mainly to lower emissions.The black carbon deposition reached the highest rates during winter and autumn, declined significantly in spring and reached a minimum during the summer.

Wet and dry deposition rates have been considered separately. The dry deposition ranked in magnitude well below the wet deposition, but it was more evenly distributed. Dry deposition reached its highest rates in southern Finland. However, the

ACPD
12, 24395–24435, 2012

wet deposition remained the dominant process of removing black carbon from atmosphere during autumn, winter and spring, while in the summer the two removal mechanisms were similar in efficiency. Unfortunately, the lack of surface measurements of black carbon deposition did not allow us to properly evaluate the model performance in simulating this particular feature. Nevertheless, the model provides at least information on spatial and temporal distribution of BC concentrations and deposition, which can be used to investigate the black carbon deposition effects on snow over Finland.

In order to calculate the BC deposition on snow, information about the simulated snow depth (snow water equivalent) was used. The mass of black carbon deposited via dry and wet deposition were summed for all of the time steps in which the snow depth was over zero. Figure 14 summarizes the seasonal black carbon deposition within the snowpack for winter and spring only, as during the summer the deposition on snow was practically zero and very small during the autumn. The total deposition amount of BC in Finland was 1545.4 mg m^{-2} in the winter months (January, February and December 2005) and 496.69 mg m^{-2} in spring, corresponding to 3.6079 Gg and 1.1536 Gg, respectively, for the entire domain.

4 Summary and concluding remarks

The aim of this study was to investigate the capability of the regional climate-aerosol model REMO.-HAM to predict black carbon concentrations at various sites in Finland, with focus on Hyytiälä station. Several statistical tools were utilized in order to better evaluate the model's predictive ability. Each statistic was able to explain a certain aspect of the model and measurement comparison: the monthly-median comparison illustrated the ability of the model to reproduce the seasonal pattern of the BC measurements, the overlap coefficient of two probability density functions offered an approach for the measurement of the agreement between two distributions in any distributional setting, and the Z-score brought additional information on the shape and spread of the distributions. Together, these statistical tools generated a more complete picture

ACPD
12, 24395–24435, 2012

on the behaviour of the regional aerosol climate model REMO-HAM. In addition to the statistical tools, wind directions and precipitation data were examined.

The main results of this study are the following:

1. The model is able to simulate to a certain extent the seasonal variation of BC concentrations, especially during the spring, summer and autumn seasons.
2. Satisfactory agreement between the model and measurements based on OVL and Z-coefficients can be found for the same periods of time.
3. The model is biased low with respect to the black carbon concentrations larger than 500 ng m^{-3}.
4. The model is biased high with respect to black carbon concentrations smaller than 250 ng m^{-3}.
5. The model compares well against the source directions of high black carbon concentrations.
6. The model overestimation of precipitation is most likely only partially responsible for the underestimation of black carbon concentrations.
7. REMO-HAM simulates a large spatial and seasonal variability of black carbon concentrations and deposition rates over Finland, reflecting the emission pattern.
8. The deposition of black carbon on snow have been estimated for winter and spring 2005.

The above results indicate that the model's low bias for the black carbon concentrations is due mainly to the inaccuracy of the emission inventories, whose so called black carbon data are apparently representative for elemental carbon-like substance (Vignati et al., 2010b). In addition, the local sources of black carbon are often not taken into account in the emission databases, also leading to serious underestimations.

ACPD
12, 24395–24435, 2012

The comparison results suggest a need for the development of a more comprehensive country-specific emission inventory as well as for a detailed study of the BC removal mechanisms. These questions will be addressed in near future.

Acknowledgements. This work was supported by the Academy of Finland's Research Programme on Climate Change (FICCA) (project 140748), by the Finnish Ministry of the Environment, by Helsinki University Center for Environment HENVI, EU LIFE+ project LIFE09 ENV/FI/000572 MACEB and FCoE. Grateful acknowledgement for proofreading and correcting the English language goes to Declan O'Donnell.

References

Anttila, P., Makkonen, U., Hellén, H., Kyllönen, K., Leppänen, S., Saari, H., and Hakola, H.: Impact of the open biomass fires in spring and summer of 2006 on the chemical composition of background air in south-eastern Finland, Atmos. Environ., 42, 6472–6486, 2008. 24401

Bond, T. C., Streets, D., Yarber, K., Woo, J., and Klimont, Z.: A technology-based global inventory of black and organic carbon emissions from combustion, J. Geophys. Res. Atmos., 109, D14203, doi:10.1029/2003JD003697, 2004. 24397

Bond, T. C., Zarzycki, C., Flanner, M. G., and Koch, D. M.: Quantifying immediate radiative forcing by black carbon and organic matter with the Specific Forcing Pulse, Atmos. Chem. Phys., 11, 1505–1525, doi:10.5194/acp-11-1505-2011, 2011. 24397

Carmichael, G., Ferm, M., Thongboonchoo, N., Woo, J., Chan, L., Murano, K., P.H., V., Mossberg, C., R., B., Boonjawat, J., Upatum, P., Mohan, M., Adhikary, S., Shrestha, A., Pienaar, J., Brunke, E., Chen, T., Jie, T., Guoan, D., Peng, L., Dhiharto, S., Harjanto, H., Jose, A., Kimani, W., Kirouane, A., Lacaux, J.-P., Richard, S., Barturen, O., Cerda, J., Athayde, A., Tavares, T., Cotrino, J., and Bilici, E.: Measurements of sulfur dioxide, ozone and ammonia concentrations in Asia, Africa, and South America using passive samplers, Atmos. Environ., 37, 1293–1308, 2003. 24398

Clemons, T. and Bradley Jr., E.: A nonparametric measure of the overlapping coefficient, Comp. Stat. Dat. Anal., 34, 51–61, 2000. 24406

Cooke, W. F., Liousse, C., Cachier, H., and Feichter, J.: Construction of a 1 1 fossil fuel emission data set for carbonaceous aerosol and implementation and radiative impact in the ECHAM-4 mode, J. Geophy. Res., 104, 137–162, 1999. 24396

ACPD

12, 24395–24435, 2012

Croft, B., Lohmann, U., and von Salzen, K.: Black carbon ageing in the Canadian Centre for Climate modelling and analysis atmospheric general circulation model, Atmos. Chem. Phys., 5, 1931–1949, doi:10.5194/acp-5-1931-2005, 2005. 24398

Croft, B., Lohmann, U., Martin, R. V., Stier, P., Wurzler, S., Feichter, J., Posselt, R., and Ferrachat, S.: Aerosol size-dependent below-cloud scavenging by rain and snow in the ECHAM5-HAM, Atmos. Chem. Phys., 9, 4653–4675, doi:10.5194/acp-9-4653-2009, 2009. 24401

Decesari, S., Fuzzi, S., Facchini, M. C., Mircea, M., Emblico, L., Cavalli, F., Maenhaut, W., Chi, X., Schkolnik, G., Falkovich, A., Rudich, Y., Claeys, M., Pashynska, V., Vas, G., Kourtchev, I., Vermeylen, R., Hoffer, A., Andreae, M. O., Tagliavini, E., Moretti, F., and Artaxo, P.: Characterization of the organic composition of aerosols from Rondônia, Brazil, during the LBA-SMOCC 2002 experiment and its representation through model compounds, Atmos. Chem. Phys., 6, 375–402, doi:10.5194/acp-6-375-2006, 2006. 24398

Dentener, F., Kinne, S., Bond, T., Boucher, O., Cofala, J., Generoso, S., Ginoux, P., Gong, S., Hoelzemann, J. J., Ito, A., Marelli, L., Penner, J. E., Putaud, J.-P., Textor, C., Schulz, M., van der Werf, G. R., and Wilson, J.: Emissions of primary aerosol and precursor gases in the years 2000 and 1750 prescribed data-sets for AeroCom, Atmos. Chem. Phys., 6, 4321–4344, doi:10.5194/acp-6-4321-2006, 2006. 24401

Engler, C., Lihavainen, H., Komppula, M., Kerminen, V., Kulmala, M., and Viisanen, Y. Continous measurements of aerosol properties at the Baltic Sea, Tellus B, 59, 728–741, 2007. 24401

Furutani, H., Dallosto, M., Roberts, G., and Prather, K.: Assessment of the relative importance of atmospheric aging on CCN activity derived from field observations, Atmos. Environ., 42, 3130–3142, 2008. 24398

Gilardoni, S., Vignati, E., and Wilson, J.: Using measurements for evaluation of black carbon modeling, Atmos. Chem. Phys., 11, 439–455, doi:10.5194/acp-11-439-2011, 2011. 24398

Hansen, J. and Nazarenko, L.: Soot climate forcing via snow and ice albedos, P. Natl. Acad. Sci. USA, 101, 423–428, 2004. 24396

Hansen, J., Sato, M., and Ruedy, R., Nazarenko, L., Lacis, A., Schmidt, G. A. and Russell, G., Aleinov, I., Bauer, M., Bauer, S., Bell, N., Cairns, B., Canuto, V., Chandler, M., Cheng, Y., Del Genio, A. , Faluvegi, G., Fleming, E., Friend, A., Hall, T., Jackman, C., Kelley, M., Kiang, N., Koch, D., Lean, J., Lerner, J., Lo, K., Menon, S., Miller, R., Minnis, P., Novakov, T., Oinas, V., Perlwitz, Ja., Perlwitz, Ju. , Rind, D., Romanou, A., Shindell, D., Stone, P., Sun, S., Tausnev,

ACPD
12, 24395–24435, 2012

N., Thresher, D., Wielicki, B., Wong, T., Yao, M., and Zhang, S.: Efficacy of climate forcings, J. Geophys. Res., 110, D18104, doi:10.1029/2005JD005776, 2005. 24397
Hari, P. and Kulmala, M.: Station for Measuring Ecosystem-Atmosphere Relations (SMEAR II), Boreal Env. Res., 10, 315–322, 2005. 24401
Hart, A.: Mann-Whitney test is not just a test of medians: differences in spread can be important, BMJ, 323, 391–393, doi:10.1136/bmj.323.7309.391, 2001. 24408
Hatakka, J., Aalto, T., Aaltonen, V., Aurela, M., Hakola, H., Komppula, M., Laurila, T., Lihavainen, H., Paatero, J., Salminen, K., and Viisanen, Y.: Overview of the atmospheric research activities and results at Pallas GAW station, Boreal Environ. Res., 8, 365–384, 2003. 24401
Haywood, J. M. and Shine, K. P.: The effect of anthropogenic sulfate and soot aerosol on the clear sky planetary radiation budget, Geophys. Res. Lett, 22, 603–606, 1995. 24398
Hyvärinen, A.-P., Kolmonen, P., Kerminen, V.-M. V., Virkkula, A., Leskinen, A., Komppula, M., Hatakka, J., Burkhart, J., Stohl, A., Aalto, P., Kumala, M., Lehtinen, K., Viisanen, Y., and Lihavainen, H.: Aerosol black carbon at five background measurement sites over Finland, a gateway to the Arctic, Atmos. Environ., 45, 4042–4050, 2011. 24401, 24402, 24405
Jacob, D.: A note to the simulation of the annual and inter-annual variability of the water budget over the Baltic Sea drainage basin, Meteorol. Amtos. Phys., 77, 61–73, 2001. 24400
Jacob, D. and Podzun, R.: Sensitivity Studies with the Regional Climate Model REMO, Meteorol. Atmos. Phys., 63, 119–129, 1996. 24400
Jacobson, M. Z.: Climate response of fossil fuel and biofuel soot, accounting for soot's feedback to snow and sea ice albedo and emissivity, J. Geophys. Res., 109, D21201, doi:10.1029/2004JD004945, 2004. 24396, 24397
Jones, P., Harris, I., and of East Anglia Climatic Research Unit (CRU): CRU Time Series (TS) high resolution gridded datasets, available at: http://badc.nerc.ac.uk/view/badc.nerc.ac.uk__ATOM__dataent_1256223773328276, 2008. 24410
Junninen, H., Lauri, A., Keronen, P., Aalto, P., Hiltunen, V., Hari, P., and Kulmala, M.: SmartSMEAR: on-line data exploration and visualization tool for SMEAR stations, Boreal Environ. Res., 14, 447–457, 2009. 24409
Koch, D., Schulz, M., Kinne, S., McNaughton, C., Spackman, J. R., Balkanski, Y., Bauer, S., Berntsen, T., Bond, T. C., Boucher, O., Chin, M., Clarke, A., De Luca, N., Dentener, F., Diehl, T., Dubovik, O., Easter, R., Fahey, D. W., Feichter, J., Fillmore, D., Freitag, S., Ghan, S., Ginoux, P., Gong, S., Horowitz, L., Iversen, T., Kirkevåg, A., Klimont, Z., Kondo, Y., Krol, M., Liu, X., Miller, R., Montanaro, V., Moteki, N., Myhre, G., Penner, J. E., Perlwitz, J., Pitari,

ACPD
12, 24395–24435, 2012

G., Reddy, S., Sahu, L., Sakamoto, H., Schuster, G., Schwarz, J. P., Seland, Ø., Stier, P., Takegawa, N., Takemura, T., Textor, C., van Aardenne, J. A., and Zhao, Y.: Evaluation of black carbon estimations in global aerosol models, Atmos. Chem. Phys., 9, 9001–9026, doi:10.5194/acp-9-9001-2009, 2009. 24398

Kulmala, M., Hämeri, K., Aalto, P. P., Mäkelä, J. M., Pirjola, L., Nilsson, E. D., Buzorius, G., Rannik, Ü., Dal Maso, M., Seidl, W., Hoffmann, T., Janson, R., Hansson, H.-C., Viisanen, Y., Laaksonen, A., and O'Dowd, C. D.: Overview of the international project on biogenic aerosol formation in the boreal forest (BIOFOR), Tellus B, 53, 324–343, 2001. 24401

Leskinen, A., Portin, H., Komppula, M., Miettinen, P., Arola, A., Lihavainen, H., Hatakka, J., Laaksonen, A., and Lehtinen, K.: Overview of the research activities and results at Puijo semi-urban measurement station, Boreal Environ. Res., 14, 576–590, 2009. 24401

Levy, H., Schwarzkopf, D., Horowitz, L., Ramaswamy, V., and Findell, K.: Strong sensitivity of late 21st century climate to projected changes in short-lived air pollutants, J. Geophys. Res.-Atmos., 113, D06102, doi:10.1029/2007JD009176, 2008. 24397

Louis, J.-F.: A parametric model of vertical eddy fluxes in the atmosphere, Bound. Lay. Meteorol., 17, 187–202, 1979. 24401

Mellor, B. and Yamada, T.: A hierarchy of turbulence closure models for planetary boundary layers., J. Atmos. Sci., 31, 1791–1806, 1974. 24401

Nordeng, T.: Extended versions of the convective parametrization scheme at ECMWF and their impact on the mean and transient activity of the model in Tropics., Tech. rep., ECMWF, Shineld Park, Reading, RG2 9AX, United Kingdom, 1994. 24401

Pietikäinen, J.-P., O'Donnell, D., D., Teichmann, C., Karstens, U., Pfeifer, S., Kazil, J., Podzum, R., Rast, S., Fiedler, S., Kokkola, H., Birmili, W., O'Dowd, C., Baltensperger, U., Weingartner, E., Gehrig, R., Spindler, G., Kulmala, M., Feichter, J., Jacob, D., and Laaksonen, A.: Implementation of the HAM-M7 aerosol module and ECHAM5 cloud physics in the regional model REMO, Geosci. Model Dev. Discuss., in preparation, 2012. 24400, 24401

Pöschl, U.: Atmospheric Aerosols: Composition, Transformation, Climate and Health Effects, Angewandte Chemie International Edition, 44, 7520–7540, doi:10.1002/anie.200501122, 2005. 24398

Ramanathan, V. and Carmichael, G.: Global and regional climate changes due to black carbon, Nature Geosci., 1, 221–227, 2008. 24397

Roeckner, E., Arpe, K., Bengtsson, L., Christoph, M., Claussen, M. andDumenil, L., Esch, M., Schlese, U., and Schulzweida, U.: The atmospheric general circulation model ECHAM4:

ACPD
12, 24395–24435, 2012

Model description and simulation of present-day climate., Tech. Rep. 218, Max Planck Institute for Meteorology, 1996. 24400

Roeckner, E., Baeuml, G., Bonventura, L., Brokopf, R., Esch, M., Giorgetta, M., Hagemann, S., Kirchner, I., Kornblueh, L., Manzini, E., Rhodin, A., Schlese, U., Schulzweida, U., and Tompkins, A.: The atmospheric general circulation model ECHAM5. PART I: Model description., Tech. Rep. 349, Max Planck Institute for Meteorology, 2003. 24400

Schwarz, J., Spackman, J., Gao, R., Watts, L., Stier, P., Schulz, M., Davis, S., Wofsy, S. C., and Fahley, D.: Global scale black carbon profiles observed in the remote atmosphere and compared to models, Geophys. Res. Lett., 37, L118812, doi:10.1029/2010GL044372, 2010. 24398

Smolarkiewicz, P. K.: Simple positive definite advection scheme with small implicit diffusion, Mon. Weather Rev., 111, 479–486, 1983. 24401

Smolarkiewicz, P. K.: A fully multidimensional positive definite advection transport algorithm with small implicit diffusion., J.Comput. Phys., 54, 325–362, 1984. 24401

Solmon, F., Giorgi, F., and Liousse, C.: Aerosol modelling for regional climate studies: application to anthropogenic particles and evaluation over a European/African domain, Tellus, 58B, 51–72, 2006. 24398

Stier, P., Feichter, J., Kinne, S., Kloster, S., Vignati, E., Wilson, J., Ganzeveld, L., Tegen, I., Werner, M., Balkanski, Y., Schulz, M., Boucher, O., Minikin, A., and Petzold, A.: The aerosol-climate model ECHAM5-HAM, Atmos. Chem. Phys., 5, 1125–1156, doi:10.5194/acp-5-1125-2005, 2005. 24398, 24400, 24401, 24420

Tegen, I., Hollrig, P., Chin, M., Fung, I., Jacob, D., and Penner, J.: Contribution of different aerosol species to the global aerosol extinction optical thickness, J. Geophy. Res., 102, 23895–23915, 1997. 24398

Textor, C., Schulz, M., Guibert, S., Kinne, S., Balkanski, Y., Bauer, S., Berntsen, T., Berglen, T., Boucher, O., Chin, M., Dentener, F., Diehl, T., Easter, R., Feichter, H., Fillmore, D., Ghan, S., Ginoux, P., Gong, S., Grini, A., Hendricks, J., Horowitz, L., Huang, P., Isaksen, I., Iversen, I., Kloster, S., Koch, D., Kirkevåg, A., Kristjansson, J. E., Krol, M., Lauer, A., Lamarque, J. F., Liu, X., Montanaro, V., Myhre, G., Penner, J., Pitari, G., Reddy, S., Seland, Ø., Stier, P., Takemura, T., and Tie, X.: Analysis and quantification of the diversities of aerosol life cycles within AeroCom, Atmos. Chem. Phys., 6, 1777–1813, doi:10.5194/acp-6-1777-2006, 2006. 24398

ACPD

12, 24395–24435, 2012

Tiedtke, M.: A comprehensive mass flux scheme for cumulus parameterization in large-scale models, Mon. Weather Rev., 117, 1779–1800, 1989. 24401

Uno, I., Carmichael, G. R., Streets, D., Satake, S., Takemura, T., Woo, J., Uematsu, M., and Ohta, S.: Analysis of surface black carbon distributions during ACE-Asia using a regional-scale aerosol model, J. Geophy. Res., 108, 8636, doi:10.1029/2002JD003252, 2003. 24398

Vignati, E., Wilson, J., and Stier, P.: M7: An efficient size-resolved aerosol microphysics module for large-scale aerosol transport models, J. Geophys. Res., 109, D22202, doi:10.1029/2003JD004485, 2004. 24400

Vignati, E., Facchini, M. C., Rinaldi, M., Scanell, C., Ceburnis, D., Sciare, J., Kanakidou, M., Myriokefalitakis, S., and O'Dowd, C. D.: Global scale emission and distribution of sea spray aerosol: sea-salt and organic enrichment, Atmos. Environ., 44, 670–677, 2010a. 24398

Vignati, E., Karl, M., Krol, M., Wilson, J., Stier, P., and Cavalli, F.: Sources of uncertainties in modelling black carbon at the global scale, Atmos. Chem. Phys., 10, 2595–2611, doi:10.5194/acp-10-2595-2010, 2010b. 24397, 24413

Williams, J., Crowley, J., Fischer, H., Harder, H., Martinez, M., Petäjä, T., Rinne, J., Bäck, J., Boy, M., Dal Maso, M., Hakala, J., Kajos, M., Keronen, P., Rantala, P., Aalto, J., Aaltonen, H., Paatero, J., Vesala, T., Hakola, H., Levula, J., Pohja, T., Herrmann, F., Auld, J., Mesarchaki, E., Song, W., Yassaa, N., Nölscher, A., Johnson, A. M., Custer, T., Sinha, V., Thieser, J., Pouvesle, N., Taraborrelli, D., Tang, M. J., Bozem, H., Hosaynali-Beygi, Z., Axinte, R., Oswald, R., Novelli, A., Kubistin, D., Hens, K., Javed, U., Trawny, K., Breitenberger, C., Hidalgo, P. J., Ebben, C. J., Geiger, F. M., Corrigan, A. L., Russell, L. M., Ouwersloot, H. G., Vilà-Guerau de Arellano, J., Ganzeveld, L., Vogel, A., Beck, M., Bayerle, A., Kampf, C. J., Bertelmann, M., Köllner, F., Hoffmann, T., Valverde, J., Gonzàlez, D., Riekkola, M.-L., Kulmala, M., and Lelieveld, J.: The summertime Boreal forest field measurement intensive (HUMPPA-COPEC-2010): an overview of meteorological and chemical influences, Atmos. Chem. Phys., 11, 10599–10618, doi:10.5194/acp-11-10599-2011, 2011. 24403

Wu, J., Jiang, W., Fu, C., Su, B., Liu, H., and Tang, J.: Simulation of the radiative effect of black carbon aerosols and the regional climate response over China, Adv. Atmos. Sci., 21, 637–649, 2004. 24398

Wu, J., Fu, C., Xu, Y., Tang, J., Wang, W., and Wang, Z.: Simulation of direct effects of black carbon aerosol and temperature and hydrological cycle in Alia by a Regional Climate Model, Meteorol. Atmos. Phys., 100, 179–193, doi:10.1007/s00703-008-0302-y, 2008. 24399

ACPD
12, 24395–24435, 2012

Table 1. The modal structure of HAM-M7. N_i denotes the aerosol number of mode i and M_i^j denotes the mass of compound j. The dry radius r shows the limits of different modes (Stier et al., 2005).

Mode	Soluble/Mixed	Insoluble
Nucleation mode $r \leq 5$ nm	N_1, M_1^{S}	
Aitken mode 5 nm $< r \leq 50$ nm	N_2, M_2^{S}, M_2^{BC}, M_2^{POM}	N_5, M_5^{BC}, M_5^{POM}
Accumulation mode 50 nm $< r \leq 0.5$ µm	N_3, M_3^{S}, M_3^{BC}, M_3^{POM}, M_3^{SS}, M_3^{DU}	N_6, M_6^{DU}
Coarse mode $r > 0.5$ µm	N_4,M_4^{S}, M_4^{BC}, M_4^{POM}, M_4^{SS}, M_4^{DU}	N_7, M_7^{DU}

ACPD
12, 24395–24435, 2012

Table 2. Measurement details for each station.

Station	Instrument	Inlet	Inlet height (ground/sea level)	Measurements started
Pallastunturi	Aethalometer AE 31*	Gas line, Total Air	7 m/572 m	18.08.2005 07.01.2008
	MAAP	PM_{10}	7 m/572 m	04.09.2007
Hyytiälä	Aethalometer AE 31	PM_{10}	4 m/179 m	08.12.2004
Puijo	MAAP	$PM_{2.5}$	75 m/306 m	25.08.2006
Utö	Aethalometer AE 31	$PM_{2.5}$	2 m/7 m	11.01.2007
Virolahti	Aethalometer AE 31	$PM_{2.5}$	2 m/4 m	26.08.2006

* In the Total Air Inlet since 7 January 2008. Gas line inlet has a cut-off size of about 7 µm. Total air inlet has no cut-off, and has heating for drying the aerosol.

ACPD
12, 24395–24435, 2012

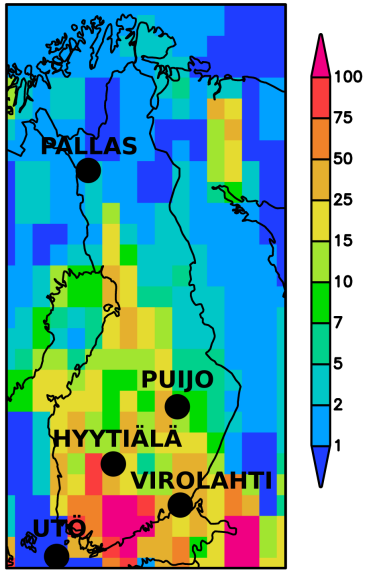

Fig. 1. . The location of the measurement stations in Finland. The color map represents the yearly black carbon emissions [mg m^{-2}].

ACPD
12, 24395–24435, 2012

BC concentration and deposition estimations in Finland

A. I. Hienola et al.

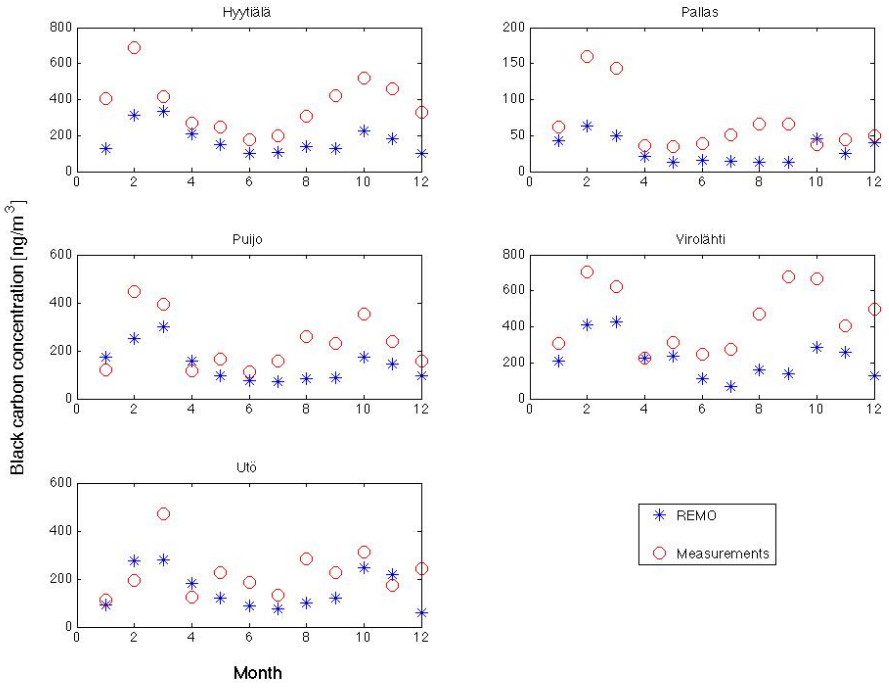

Fig. 2. Monthly average of black carbon concentrations (red circles represent the measurements and the blue stars the model result).

ACPD
12, 24395–24435, 2012

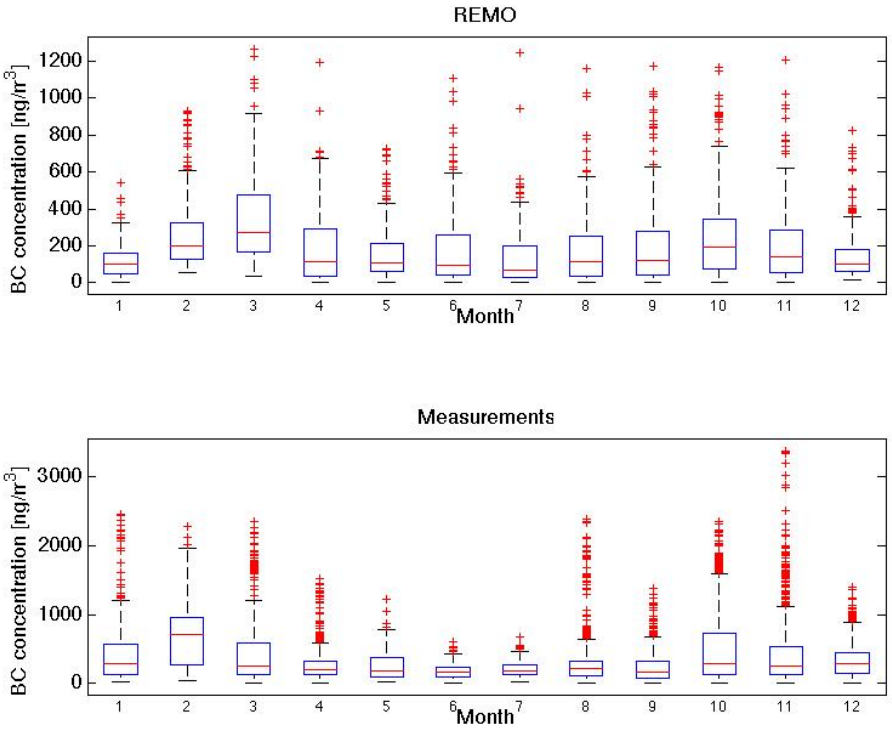

Fig. 3. The box-and-whisker diagram of the model (upper panel) and measurements (lower panel) BC concentrations in Hyytiälä. The solid red line locates the median, the edges of the boxes are the 25th and 75th percentiles and the red plus marks represent the outliers.

ACPD
12, 24395–24435, 2012

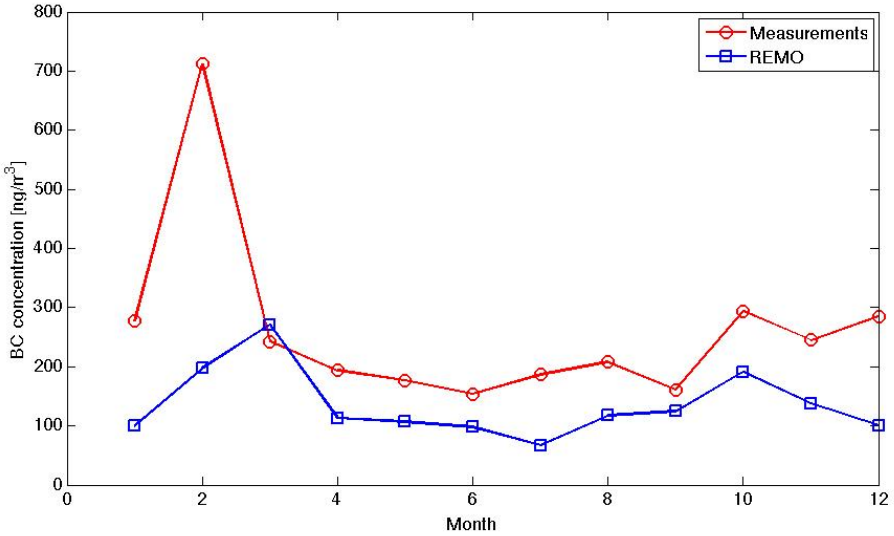

Fig. 4. Monthly medians of the black carbon concentrations, where the red circles represent the measurements and the blue squares the model results.

ACPD
12, 24395–24435, 2012

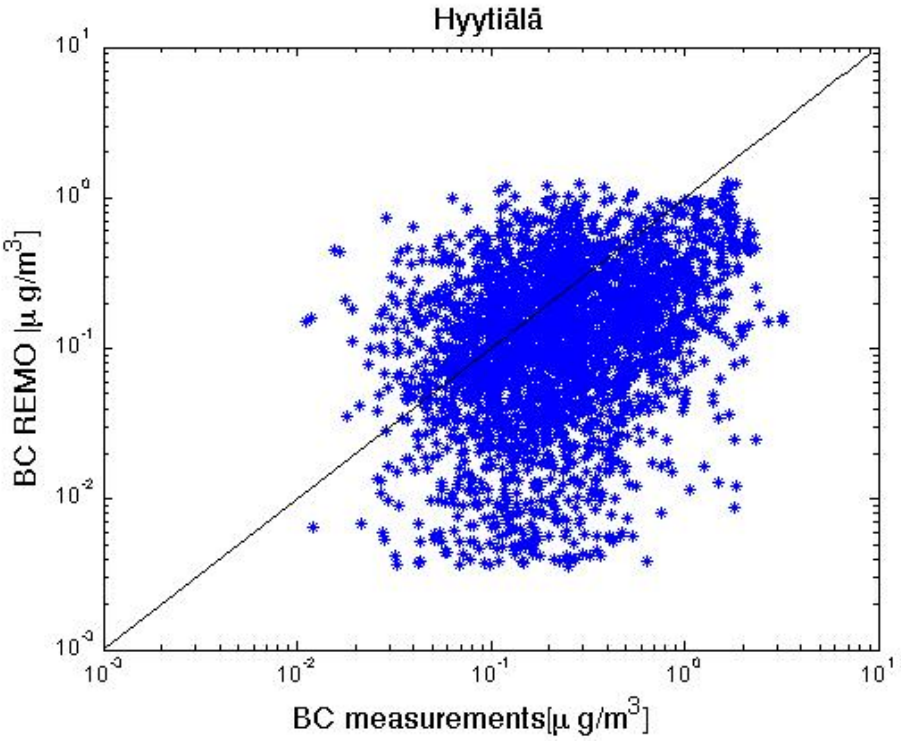

Fig. 5. 3-hourly (upper panel) scatter plot of the black carbon concentrations in Hyytiälä: measurements vs model.

ACPD
12, 24395–24435, 2012

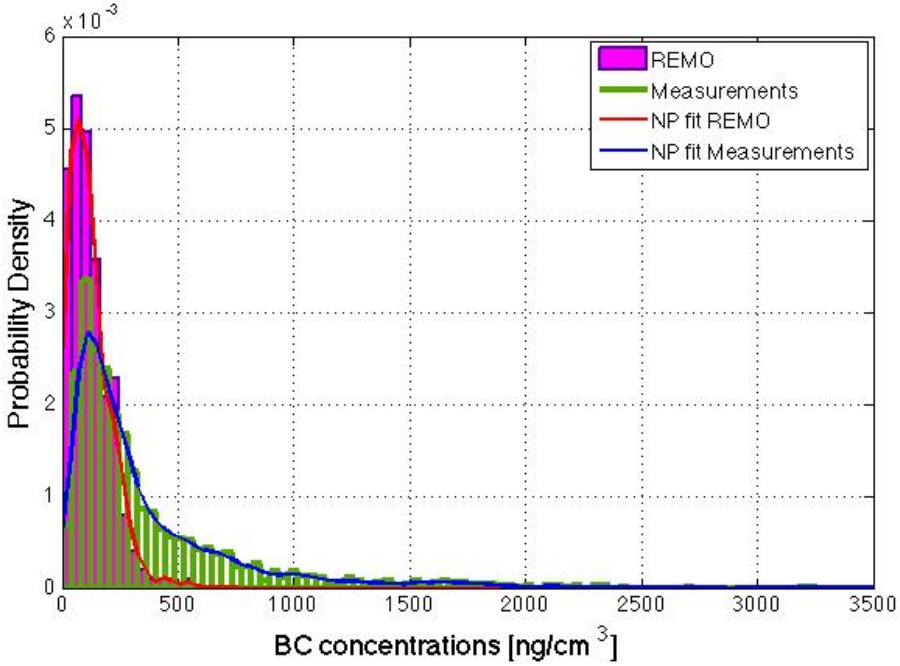

Fig. 6. The histograms (pink – REMO and green – measurements) and the probability density functions (pink – REMO and blue – measurements) of the black carbon concentration for the entire experimental period – 2005.

ACPD
12, 24395–24435, 2012

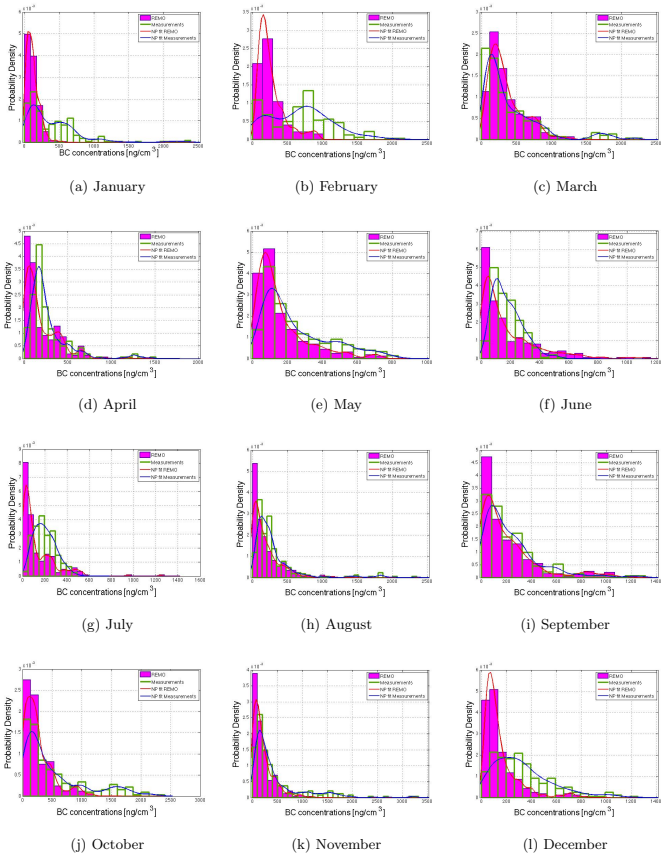

(a) January (b) February (c) March

(d) April (e) May (f) June

(g) July (h) August (i) September

(j) October (k) November (l) December

Fig. 7. Monthly histograms (pink – REMO and green – measurements) and the probability density functions (pink – REMO and blue – measurements) of the black carbon concentration.

ACPD
12, 24395–24435, 2012

BC concentration and deposition estimations in Finland

A. I. Hienola et al.

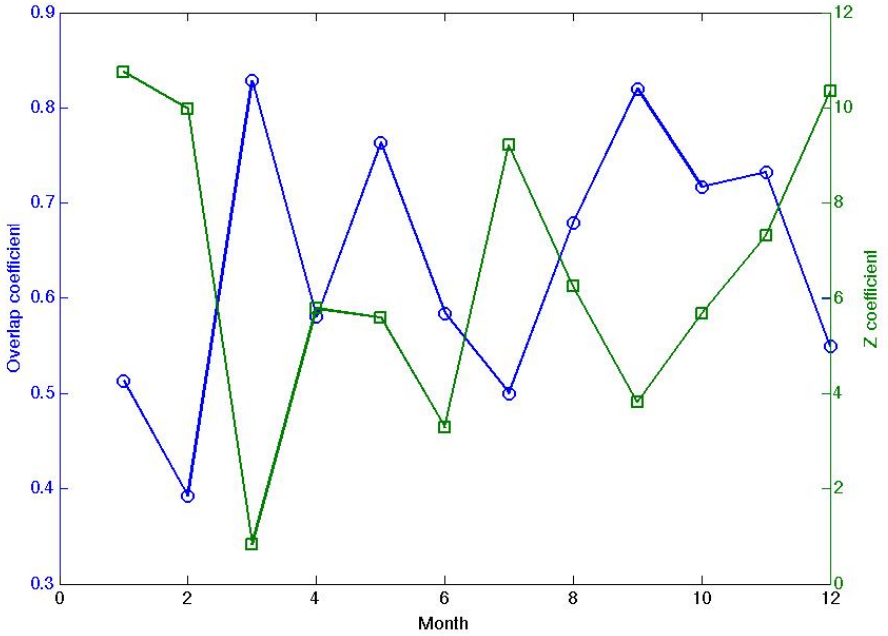

Fig. 8. Monthly overlap coefficient OVL and Z-coefficient.

ACPD
12, 24395–24435, 2012

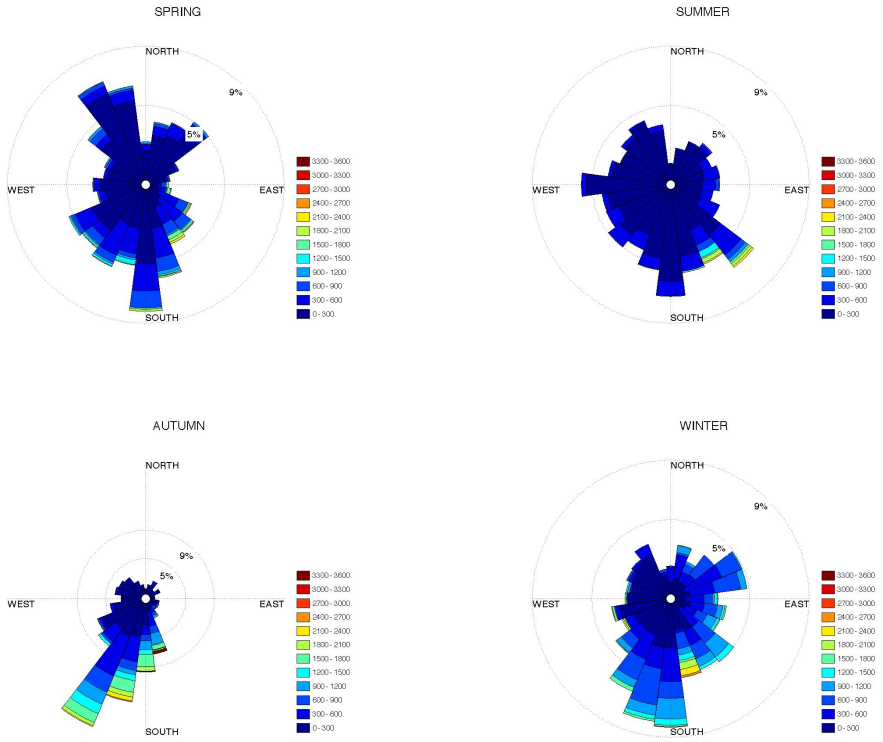

Fig. 9. The measured seasonal wind directions (slices) and BC concentrations represented as color scheme.

ACPD
12, 24395–24435, 2012

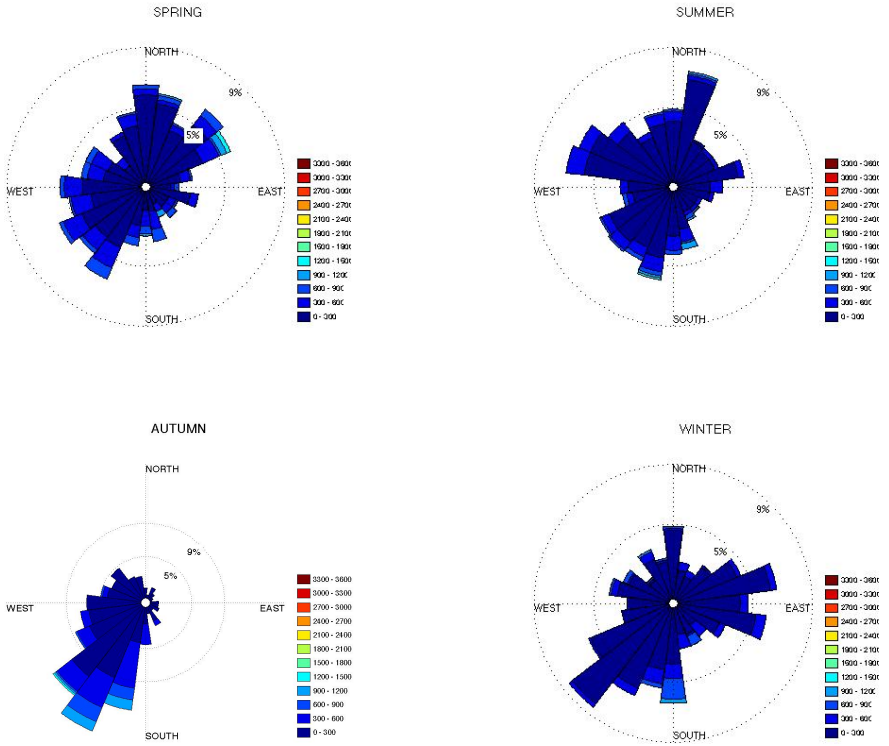

Fig. 10. The modeled seasonal wind directions (slices) and BC concentrations represented as color scheme.

ACPD
12, 24395–24435, 2012

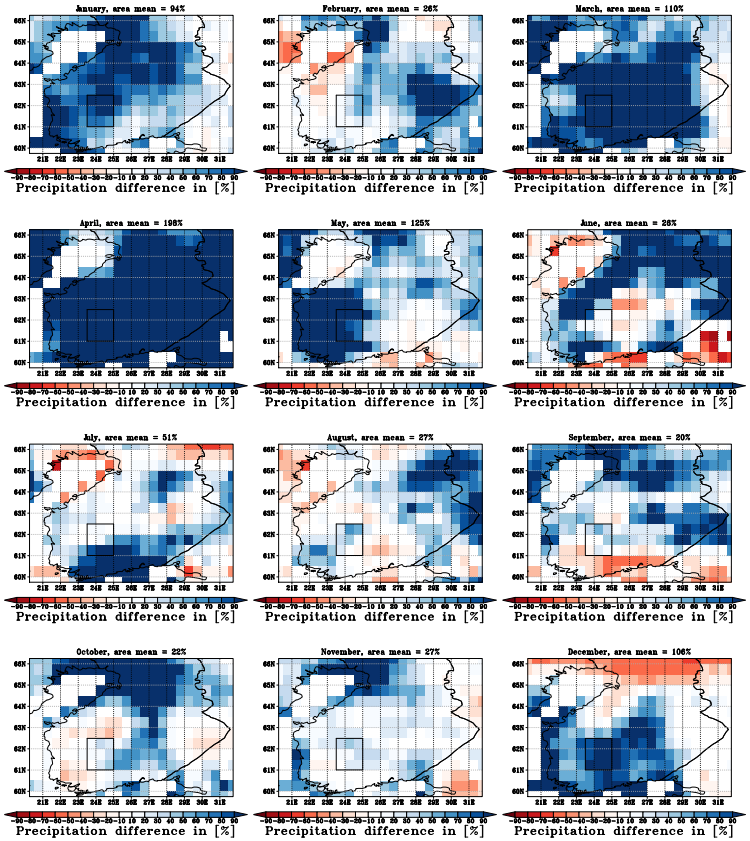

Fig. 11. Monthly percentage difference for precipitation in Southern Finland. Blue and red colors represent the model overestimation and underestimation, respectively. White represents agreement. The central grid in the outlined square indicates Hyytiälä location, while the number above each panel represents the mean precipitation difference for the square.

ACPD
12, 24395–24435, 2012

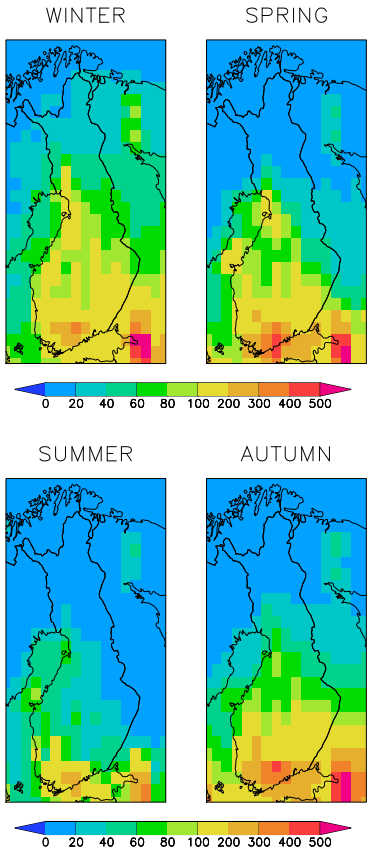

Fig. 12. Seasonal black carbon near-surface median concentration [ng m^{-3}] over Finland.

ACPD
12, 24395–24435, 2012

BC concentration and deposition estimations in Finland

A. I. Hienola et al.

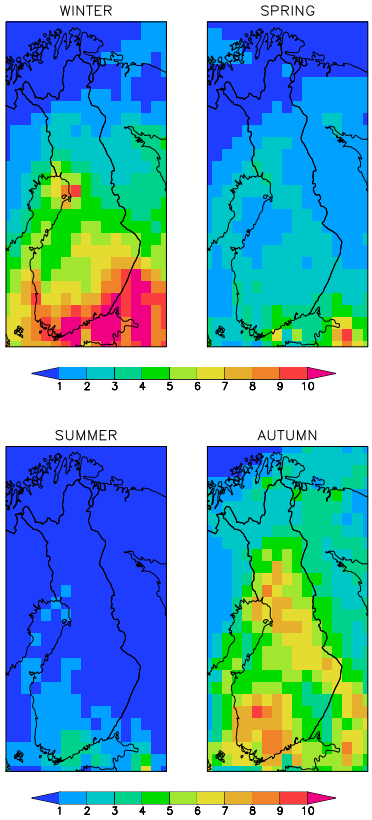

Fig. 13. Seasonal black carbon deposition fluxes [mg m^{-2}] over Finland.

ACPD
12, 24395–24435, 2012

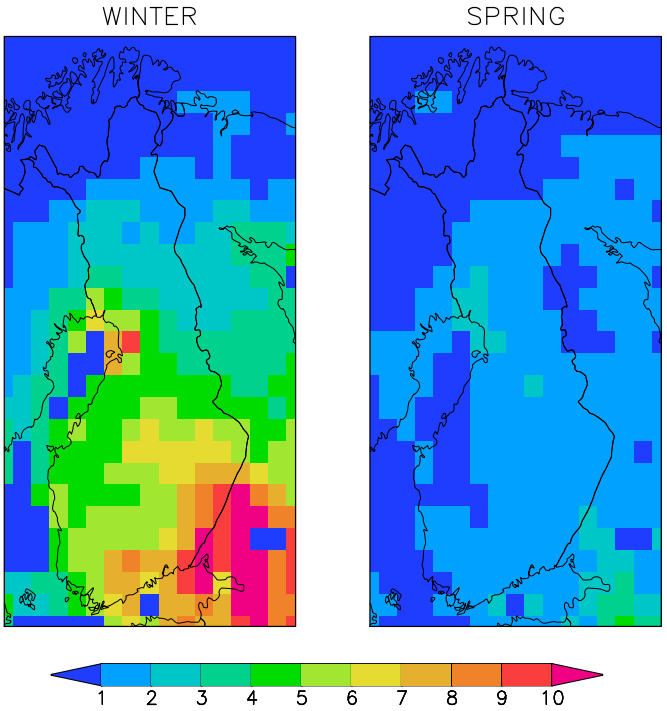

Fig. 14. Black carbon deposition flux on snow [mg^{-2}] over Finland fro winter and spring.

ACPD
12, 24395–24435, 2012

BC concentration and deposition estimations in Finland

A. I. Hienola et al.